THE JOURNAL OF PHYSICAL CHEMISTRY C

Article

Cite This: J. Phys. Chem. C 2020, 124, 309−321

pubs.acs.org/JPCC

Stabilization of Super Electrophilic Pd^{+2} Cations in Small-Pore SSZ-13 Zeolite

Konstantin Khivantsev,*[,†,∥] Nicholas R. Jaegers,[†,‡,∥] Iskra Z. Koleva,[§,∥] Hristiyan A. Aleksandrov,*[,§] Libor Kovarik,[†] Mark Engelhard,[†] Feng Gao,[†] Yong Wang,[†,‡] Georgi N. Vayssilov,[§] and Janos Szanyi*[,†,∥]

[†]Institute for Integrated Catalysis, Pacific Northwest National Laboratory, Richland, Washington 99352, United States

[‡]Voiland School of Chemical Engineering and Bioengineering, Washington State University, Pullman, Washington 99163, United States

[§]Faculty of Chemistry and Pharmacy, University of Sofia, 1126 Sofia, Bulgaria

Supporting Information

ABSTRACT: We provide the first observation and characterization of super electrophilic metal cations on a solid support. For Pd/SSZ-13, the results of our combined experimental (Fourier transform infrared spectroscopy, X-ray photoelectron spectroscopy, high-angle annular dark-field scanning transmission electron microscopy) and density functional theory study reveal that Pd ions in zeolites, previously identified as Pd^{+3} and Pd^{+4}, are, in fact, present as super electrophilic Pd^{+2} species (charge-transfer complex/ion pair with the negatively charged framework oxygens). In this contribution, we reassign the spectroscopic signatures of these species, discuss the unusual coordination environment of "naked" (ligand-free) super electrophilic Pd^{+2} in SSZ-13, and their complexes with CO and NO. With CO, nonclassical, highly positive $[Pd(CO)_2]^{2+}$ ions are formed with the zeolite framework acting as a weakly coordinating anion (ion pairs). Nonclassical carbonyl complexes also form with Pt^{+2} and Ag^+ in SSZ-13. The $Pd^{+2}(CO)_2$ complex is remarkably stable in zeolite cages even in the presence of water. Dicarbonyl and nitrosyl Pd^{+2} complexes, in turn, serve as precursors to the synthesis of previously inaccessible Pd^{+2}−carbonyl−olefin $[Pd(CO)(C_2H_4)]$ and Pd^{+2}−nitrosyl−olefin $[Pd(NO)(C_2H_4)]$ complexes. Overall, we show that the zeolite framework can stabilize super electrophilic metal (Pd) cations and show the new chemistry of the Pd/SSZ-13 system with implications for adsorption and catalysis.

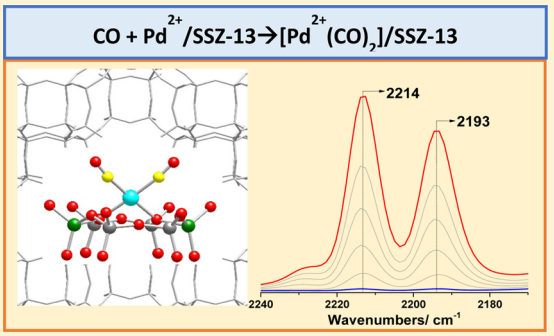

INTRODUCTION

Zeolite-supported transition metals represent an important class of catalysts, utilized extensively in the industry: from petroleum refining to emission control.[1−6] Zeolites are highly crystalline aluminosilicates with well-defined binding sites inside the microporous channels/cages of various sizes.[7] We recently demonstrated the preparation of atomically dispersed Pd (and Pt) in a small-pore zeolite SSZ-13 (Si/Al ratio of ∼ 6) with loadings of up to 2 wt % by a simple method (modified incipient wetness impregnation).[8] Previous studies suggested that harsh hydrothermal aging is required to atomically disperse Pd ions in SSZ-13 and other zeolites.[57,58] In those studies, however, the as-prepared materials initially contained a significant amount of PdO nanoparticles. Although aging was suggested to improve the metal dispersion, it does not lead to complete dispersion of Pd because of the simultaneous loss of Pd and zeolite dealumination under such harsh conditions.[60] We have also shown that Pd/SSZ-13 with atomically dispersed Pd was capable of simultaneously adsorbing NO and CO from vehicle exhaust streams with unrivaled efficiency under practical conditions (i.e., in the presence of water in the stream) at low temperatures.[8−10] The importance of their adsorption capacity lies in the fact that the current state-of-the-art selective catalytic reduction (SCR) materials[61] cannot effectively convert NOx to N_2 under practical conditions at temperatures lower than 200 °C. To circumvent this problem, Pd/SSZ-13 can be used as a low-temperature passive NOx adsorber (PNA). In this process, NOx is adsorbed at low temperature during cold start/vehicle idle and released at temperatures above 300 °C,[8] when the downstream SCR catalyst composed primarily of Cu/SSZ-13 (previously characterized extensively using various spectroscopic and density functional theory (DFT) methods)[61−63] becomes active. Their unique performance for PNA applications, coupled with their excellent hydrothermal stability, puts Pd/SSZ-13 at the forefront for low-temperature emission control applications. Furthermore, the high loading of atomically dispersed Pd serves as a perfect example to investigate and

Received: July 16, 2019
Revised: December 2, 2019
Published: December 4, 2019

DOI: 10.1021/acs.jpcc.9b06760
J. Phys. Chem. C 2020, 124, 309−321

understand the behavior of transition-metal ions in microporous materials. The high uniformity of atomically dispersed Pd ions in the micropores of this zeolite allows us to investigate the fundamentals of NOx uptake and release, and the oxidation state of the metal. Moreover, the ability to synthesize M/SSZ-13 materials with a uniform, atomic metal dispersion opens a new avenue to investigate other transition-metal ion exchange zeolites, e.g., Pt and Ag.

The oxidation state of Pd in zeolites has been considered a settled matter for the last three decades. For example, Bell and co-workers[11] concluded that Pd/ZSM-5 with a 0.44 wt % loading could be prepared by the ion exchange of oxidized Pd. The IR spectra of adsorbed CO on this sample displayed numerous bands besides the C−O stretching features of Pd^0−CO species: Pd^{+2}−CO, Pd^{+1}−CO, and even bands attributed to $Pd^{+3}(CO)_2$ were observed. Subsequently, Hadjiivanov and co-workers[12] concluded that the adsorption of CO at 100 K produces $Pd^{3+}(CO)_2$ complexes (unselectively) as well as a range of $Pd^{+2}(CO)_x$, Pd^{+1}−CO, and Pd^0−CO complexes upon warming from 100 to 298 K. These studies suggested that Pd is initially present as either Pd^{+4} or Pd^{+3} ions that are reduced to Pd^0 metal upon CO adsorption. However, as mentioned earlier, strategies employed in most previous works to produce atomically monodisperse Pd species were not successful and, as a result, both Pd ions and polynuclear PdO moieties coexisted in the micropores accompanied by larger PdO particles on the external surface. Surprisingly, only one density functional theory (DFT) study has been employed for Pd/zeolite systems, reported by us earlier.[8] Prior to our studies on Pd(Pt)/SSZ-13, high loadings of atomically dispersed metals at elevated levels (>1%) had not been attained. For example, Moliner et al. demonstrated a route to introduce 0.23 wt % atomically dispersed Pt in SSZ-13 with a Si/Al ratio of 7−9.[13] Here, we report the results of a combined spectroscopy/microscopy/computation study on a 1% Pd-loaded SSZ-13 zeolite, in which the metal ions are present in atomic dispersion. Here, we identify super electrophilic metal ions in a solid support with the help of FTIR spectroscopy (coupled with DFT calculations) and quasi in situ X-ray photoelectron spectroscopy (XPS). This latter technique showed an unprecedented 2.3 eV shift of the binding energy (BE) of Pd(II) ion upon dehydration compared to the atomically dispersed partially hydrated ion. This unusually high shift allows us to characterize super electrophilicity quantitatively: shifts higher than 2 eV upon dehydration of a partially hydrated, atomically dispersed metal cation in zeolite would mean that it forms a super electrophilic M cation. This finding can be extended to other metals in zeolites (vide infra), and efforts are underway in our group to highlight the unusual catalytic chemistry of such unique super electrophilic as well as highly electrophilic metal fragments.[64] For example, such fragments were recently shown to be exceptionally active for the homolytic activation of the C−H bond of ethylene (22 kJ/mol stronger than the methane C−H bond at room temperature) under ambient conditions.[64]

We also highlight that zeolitic confined micropore architecture is imperative for the formation of such super electrophilic species, which do not form selectively (on regular solid, nonmicroporous/nonzeolitic supports). For example, the high-lying IR bands for the complexes of CO with super electrophilic transition-metal ions (stable, e.g., $Pd(II)(CO)_2$ and $Pt(II)(CO)_2$ complexes) form in zeolites with high yields but not on many other common solid supports like alumina, zirconia, silica, etc.

The interaction of these super electrophilic Pd cations with CO results in the formation of nonclassical carbonyl complexes. Similar complexes are also observed with Pt^{2+} and Ag^+ ions in SSZ-13.

EXPERIMENTAL SECTION

Na-SSZ-13 with Si/Al = 6 and ion-exchanged twice with a 2 M NH_4NO_3 aqueous solution at 80 °C for 3 h yielded the ammonium forms of SSZ-13. NH_4-SSZ-13 was subsequently dried under ambient conditions and then at 80 °C. Samples with 0.1 and 1 wt % Pd, 1 wt % Pt, and 3 wt % Ag loadings were prepared by modified ion exchange (for Pd and Pt) with a 10 wt % $Pd(NH_3)_4(NO_3)_2$ solution (Sigma-Aldrich, 99.99%) with NH_4-SSZ-13 platinum(II) tetraamine nitrate solution, and regular ion exchange for $AgNO_3$ (99.99%) solution with H-SSZ-13 (produced by the decomposition of NH_4-SSZ-13 in air at 550 °C). More specifically, a minimum amount of the Pd(II) or Pt(II) precursor solution was added to the zeolite in the amount approximately equivalent to the total pore volume of the zeolite. The thick paste was mixed and stirred vigorously for 30 min, followed by calcination in air at 650 °C for 5 h (ramping rate 2 °C/min) in the case of Pd and 350 °C in the case of Pt. H-forms of zeolites could be used as well with identical results: in that case, Pd and Pt tetramine salts were dissolved in the minimum amount of dilute ammonium hydroxide solution (pH = 11.5), mixed with the zeolite to form a thick paste (mixed vigorously), followed by drying and calcination in air at 650 °C for Pd and 350 °C for Pt. In the case of Ag, 1 g of H-SSZ-13 was dispersed in water and stirred with ∼20 mL of a 0.1 M silver nitrate solution for 3 h; then, the sample was purified by five successive centrifugation−redispersion cycles and dried at 80 °C overnight. To avoid silver autoreduction under a high vacuum in the FTIR cell, the sample was heated to 180 °C to remove residual water from Ag/SSZ-13 as quickly as possible and then immediately cooled down prior to IR measurements.

The in situ static transmission IR experiments were conducted in a homebuilt cell housed in the sample compartment of a Bruker Vertex 80 spectrometer, equipped with an MCT detector and operated at a 4 cm^{-1} resolution. The powder sample was pressed onto a tungsten mesh, which, in turn, was mounted onto a copper heating assembly attached to a ceramic feedthrough. The sample could be resistively heated, and the sample temperature was monitored by a thermocouple spot welded onto the top center of the W grid. The cold finger on the glass bulb containing CO was cooled with liquid nitrogen to eliminate any contamination originating from metal carbonyls, while NO was cleaned with multiple freeze−pump−thaw cycles. Prior to spectrum collection, a background with the activated (annealed, reduced, or oxidized) sample in the IR beam was collected. Each spectrum reported is obtained by averaging 256 scans.

High-angle annular dark-field scanning transmission electron microscopy (HAADF-STEM) was used to probe the dispersion of Pd and Pt in the prepared samples. The analysis was performed with an FEI Titan 80−300 microscope operated at 300 kV. The instrument is equipped with a CEOS GmbH double-hexapole aberration corrector for the probe-forming lens, which allows for imaging with a 0.1 nm resolution in scanning transmission electron microscopy mode (STEM). The images were acquired with a high-angle annular

DOI: 10.1021/acs.jpcc.9b06760
J. Phys. Chem. C 2020, 124, 309−321

dark-field (HAADF) detector with an inner collection angle set to 52 mrad.

Standard NOx adsorption tests were conducted in a plug-flow reactor system with powder samples (120 mg, 60−80 mesh) loaded in a quartz tube, using a synthetic gas mixture that contained ∼200 ppm of NOx or (200 ppm of NOx, 200 ppm of CO, 3 vw% of H_2O, and 14% of O_2) balanced with N_2 at a flow rate of 310 sccm (corresponding to 330 000 h^{-1}).

All of the gas lines were heated to over 100 °C. Concentrations of reactants and products were measured by an online MKS MultiGas 2030 FTIR gas analyzer with a gas cell maintained at 191 °C. Two four-way valves were used for gas switching between the reactor and the bypass. Prior to storage testing at 100 °C, the sample was pretreated in 14% of O_2 balanced in a N_2 flow for 1 h at 550 °C and cooled to the target temperature in the same feed. The gas mixture was then switched from the reactor to the bypass, and 200 ppm of NOx was added to the mixture. Upon stabilization, the gas mixture was switched back from the bypass to the reactor for storage testing for 10 min. The sample was then heated to 600 °C at a rate of 10 °C/min to record the desorption profiles of gases in the effluent.

To further disprove the possibility of the formation of Pd(IV) species upon calcination in oxygen, we performed the following experiment. In a quartz reactor equipped with valves at both ends, ∼300 mg of 1 wt % Pd/SSZ-13 was heated in dry oxygen at 600 °C for 3 h. After cooling it down to room temperature in dry airflow, the reactor was purged with dry nitrogen. Then, we moved the reactor to a moisture- and oxygen-free glovebox without exposure to ambient air (there, the sample was also prevacuumed in the antechamber of the glovebox under a high vacuum of 10^{-5}−10^{-6} Torr). The pink powder of Pd/SSZ-13 from the reactor was then transferred into a 20 mL vial with a septum screw cap. With a syringe, a 1 mL gas-phase sample from that vial was injected in the gas chromatography (GC). The analysis of the gas phase confirmed the absence of any oxygen.

Then, through the septum, we introduced a small amount of pure deaerated H_2O into the vial containing the dry dehydrated catalyst. The sample turned yellow, characteristic of hydrated Pd(II) ions. If during the interaction with water, the reduction of Pd(IV) to Pd(II) were indeed to take place, then the following redox reaction would occur: Pd(IV) + 2e → Pd(II). If Pd accepts two electrons, water has to give electrons, which can only occur via $H_2O - 2e \rightarrow 2H^+ + 1/2O_2$. If Pd(IV) were indeed reduced to Pd(II), this process would produce 14 micromoles of O_2. In the ∼20 mL vial, this amount of oxygen would be equivalent to ∼0.3% of oxygen by volume easily detectable with a GC. We injected 1 mL of the gas phase from the closed vial (after water exposure) and observed no oxygen in the gas phase. Thus, no oxygen was produced, and no Pd(IV) was formed during Pd/SSZ-13 heating in oxygen.

X-ray absorption spectroscopy (XAS) spectra were collected at X-ray beamline 9-1 of the Argonne National Laboratory. The storage ring electron energy was 7 GeV, and the ring current was in the range of 495−500 mA. Prior to these measurements, each powder sample was loaded into a cell. The XAS data were collected in the fluorescence mode. Samples were scanned at energies near the Pd K absorption edge (24 350 eV). Standards PdO, Pd foil, and $K_2[PdCl_6]$ were scanned as well. PdO and $K_2[PdCl_6]$ were mixed with BN prior to scanning. A 1 wt % Pd/SSZ-13 sample in Figure S1 was calcined in air in the XAS cell at 350 °C for 1 h, then cooled down in the airflow, and X-ray absorption near-edge structure (XANES) was recorded at room temperature.

X-ray photoelectron spectroscopy (XPS) experiments were performed using a Physical Electronics Quantera scanning X-ray microprobe. This system uses a focused monochromatic Al Kα X-ray (1486.7 eV) source for excitation and a spherical section analyzer. The instrument has a 32-element multi-channel detection system. The 80 W X-ray beam focused on a 100 μm diameter was rastered over a 1.1 × 0.1 mm rectangle on the sample. The X-ray beam was incident normal to the sample, and the photoelectron detector was at 45° off-normal. High-energy resolution spectra were collected using a pass energy of 69.0 eV with a step size of 0.125 eV. Note that the samples experienced variable degrees of charging. Low-energy electrons at ∼1 eV, 20 μA and low-energy Ar^+ ions were used to minimize this charging. First, the 0.1 and 1 wt % Pd samples were measured as is. The samples then were heated in 10% of O_2/He for 1 h at 600 °C (ramping rate 10 °C/min), followed by cooling down in O_2/He to room temperature in a flow cell attached to the XPS system. The pretreated samples were immediately transferred into the UHV chamber without exposure to the open air for the first XPS analysis. Note that following the heating treatment, adventitious carbon, ideal for binding energy (BE) calibration, became absent. Therefore, all binding energies were referenced to a Si 2p BE of SSZ-13 of 102.7 eV.

DFT calculations were performed using the PW91 exchange−correlation functional with dispersion correction (PW91-D2). Vienna ab initio simulation package (VASP) was employed for these calculations. Ultrasoft pseudopotentials were used as implemented in the VASP package. The large size of the unit cell allowed us to sample the Brillouin zone using the Γ point only. A plane-wave basis was used with a cutoff energy of 400 eV.

The monoclinic unit cell of the CHA framework consists of 36 T atoms. It was optimized for the pure silicate structure with dimensions: $a = b = 13.675$ Å, $c = 14.767$ Å; $\alpha = \beta = 90°$, $\gamma = 120°$. More details are provided in the Supporting Information (SI).

RESULTS AND DISCUSSION

After calcination in O_2 (at 400 °C), the K-edge extended X-ray absorption fine structure (EXAFS) (XANES region) of our atomically dispersed 1% Pd in SSZ-13 showed that all Pd is in the +2 oxidation state.[8] A comparison of the XANES region of the Pd/SSZ-13 spectrum with those of PdO, $[Pd(NH_3)_4](NO_3)_2$, and standard $[Pd(IV)Cl_6]^{2-}$ clearly shows the absence of Pd(IV) species within the margin of EXAFS sensitivity (Figure S1). The only other stable compounds in which Pd^{+4} and Pd^{+3} are known to exist are $Zn_2Pd(IV)O_4$ and $LaPd(III)O_3$ produced by high-temperature, high-pressure, solid-state synthesis. The XANES region K-edge features of these compounds are caused by the splitting of the d-levels of Pd^{+4} and Pd^{+3} in the octahedral crystal field, dissimilar to Pd/SSZ-13 calcined in air.[14] A series of FTIR spectra collected from our atomically dispersed 1 wt % Pd/SSZ-13 sample upon dosing CO at 298 K are displayed in Figure 1. (The cryo-HAADF-STEM images for this sample, confirming atomic dispersion of Pd, are provided in the SI (Figure S2).)

Upon CO adsorption at room temperature, well-defined absorption bands develop. The major doublet bands are centered at 2214 and 2193 cm^{-1}. Minor features at 2148 and 2110 cm^{-1} belong to CO on ionic Pd^{+2} species (see Tables S1

DOI: 10.1021/acs.jpcc.9b06760
J. Phys. Chem. C 2020, 124, 309−321

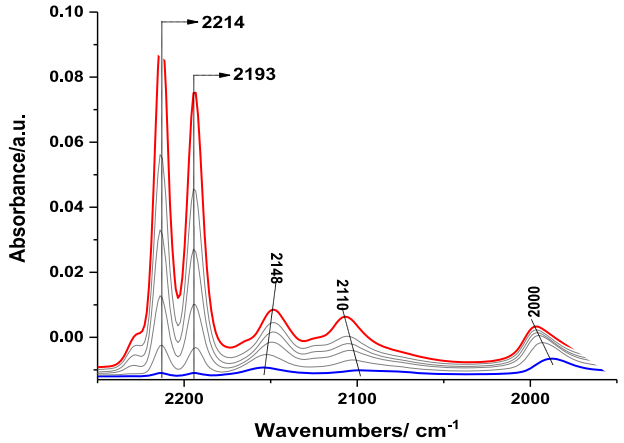

Figure 1. FTIR spectra of adsorbed CO at 298 K on 1 wt % Pd/SSZ-13 with Si/Al = 6 (CO was introduced into the IR cell in a stepwise fashion; $P(CO)_{max}$ ~5 Torr); the lines between the blue spectrum (first CO pulse) and the red spectrum (final state) indicate the sequential adsorption of approximately equal aliquots of CO until the desired CO amount is dosed on the sample (spectra are presented in a similar fashion throughout the text). Please note that we chose 1 wt % Pd/SSZ-13 with Si/Al = 6 as a model for our study due to the high uniformity of atomically dispersed Pd(II) species that are stabilized selectively as Pd(II)/2Al by the proximal Al sites. We have also explored the effect of the Si/Al ratio on the speciation and FTIR during CO adsorption on Pd/SSZ-13 with the same Pd loading (1 wt %) and varied the Si/Al ratios of 12 and 30 (Figures S33 and S34; the discussion regarding the effect of the Si/Al ratio on the Pd speciation and uniformity is in the captions of Figures S33 and S34).

and S2 for DFT confirmation). The bands at 2090 cm^{-1} and below represent CO bound to metallic Pd. Aleksandrov et al.[15,16] demonstrated for Pt clusters that the decrease in coordination number (CN) by 1 corresponded to a downshift of approx. ~7 cm^{-1} in agreement with the experimental studies.[17] The fact that the metallic ~1990 cm^{-1} band lies below that of larger (>3 nm) Pd nanoparticles (~2090 cm^{-1}) means that small Pd_4−Pd_6 clusters are present and possibly formed during CO adsorption. To further confirm this observation, part of the Pd was reduced in situ with CO at 400 °C prior to CO adsorption. The IR spectra showed an increase in the intensity of the 1990 cm^{-1} band. Upon vacuum-induced desorption, the center of this band red-shifted due to the elimination of dipole−dipole coupling interactions present at higher coverages (Figure S3). As such, we ascribe the peak at ~1990 cm^{-1} to CO adsorbed linearly on small Pd clusters, whereas bands below 1900 cm^{-1} represent doubly and possibly triply bridged CO on such clusters that are formed in small amounts (<0.5% of total Pd). Note that in agreement with works by Stair and co-workers[42] and Hadjiivanov and co-workers,[43] the molar extinction coefficients of CO bands for CO-containing species dramatically increase as the υ_{CO} goes down. For example, for metallic Pt-bound CO, it was found that the 2090 cm^{-1} band has >8 times higher molar extinction coefficient than the 2110 cm^{-1} belonging to ionic Pt.

The 2214 and 2193 cm^{-1} bands belong to ν_{C-O} vibrations previously assigned to $Pd(III)(CO)_2$ complexes by the Bell group[11] and later Hadjiivanov group[12] on Pd/ZSM-5. Unlike those systems in which the CO adsorption produced a wealth of species, in our 1 wt % Pd/SSZ-13 (Si/Al = 6), these species are formed selectively (>90%) at room temperature. These $Pd(CO)_2$ species are stable in the presence of CO, O_2, or inert atmosphere and fully decompose only above 140 °C. This means that the high uniformity of Pd in small-pore SSZ-13 enables the selective production of this species. Indeed, the symmetric and asymmetric CO bands grow and, upon evacuation, disappear in concert (Figures 1 and S3), suggesting that they belong to the same species. The assignment of these bands to dicarbonyls of Pd is further confirmed by the isotopic labeling of the adsorbate (^{13}CO) (Figure S4). In contrast, the stabilization of the Pd^{+3} in zeolite would require at least three Al atoms in either 6-membered or 8-membered rings of the SSZ-13 structure (which is highly unlikely) or Pd^{+3}−OH fragment held by two proximal Al atoms. To explain the observed high wavenumbers, we modeled unique $Pd^{4+}(CO)_2(O)$ and $Pd^{3+}(CO)_2(OH)$ complexes (Tables 1

Table 1. Binding Energies of the Neutral Ligands (in kJ/mol), Vibrational Frequencies of Diatomic Ligands ν (L) in cm^{-1}, and Number of the Unpaired Electrons in the Systems, N_s for the Select Pd Carbonyl Complexes[a]

structures	BE	BE_{L1}	BE_{L2}	ν (L)[a]	N_s
Pd^+					1
$Pd^+(CO)$	−158			2075	1
$Pd^+(CO)_2$	−252	−94		2103; 2063	1
$Pd^+(CO)_3$	−273	−20		2098; 2058; 2055	1
Pd^{2+}					0
$Pd^{2+}(CO)$	−87			2114	0
$Pd^{2+}(CO)_2$	−215	−128		2172; 2138	0
$Pd^{2+}(CO)_3$					
$Pd^{2+}(CO)_{4zeo}$	−271			2178; 2133; 2122; 1845	0
$Pd^0(CO)_{4desorbed}$				2119; 2073; 2068; 2012	
$Pd^{2+}(CO)(OH)$		−187		2121	0
$Pd^{2+}(CO)_2(OH)$		−262		2165; 2125	0
$Pd^{2+}(CO)(C_2H_4)$	−209	−151	−98	2140	0
$Pd^{3+}(CO)(OH)$		−117		2158	1
$Pd^{3+}(CO)_2(OH)$		−160		2141; 2114	1
$Pd^{4+}(CO)_2(O)$	0				
$Pd^{2+}(O)Pd^{2+}$					0
$Pd^{2+}(CO)(O)$ $Pd^{2+}(CO)$	−321			2132/2116	0

[a]All considered structures are summarized in Table S1, not shown in Table 1 for brevity.

and S1). In the case of $Pd^{4+}(CO)_2(O)$, the spontaneous formation and desorption of carbon dioxide are observed. The calculated vibrational frequencies of the other complex, $Pd^{3+}(CO)_2(OH)$, were notably lower than 2200 cm^{-1}: 2141 and 2114 cm^{-1}. The structure of Pd(IV) was more stable with 0 unpaired electrons, and for this reason, we included it. In that case, CO_2 molecule leaves the complex. These results do not agree with the experimental data. Additionally, $Pd^{+1}(CO)_2$ complex (one unpaired electron) has calculated symmetric and asymmetric C−O stretching vibrations at 2103 and 2063 cm^{-1}, significantly lower than the observed values.

The positions of the IR features for the $Pd^{2+}(CO)_2$ complex (2214 and 2193 cm^{-1}) lie at much higher values than gas-phase CO (by 61 and 50 cm^{-1}, correspondingly), suggesting the identity of a nonclassical Pd carbonyl [$Pd(CO)_2$] with essentially no back-donation from Pd to CO.[19] For an otherwise classical $Pd(CO)_2$ complex with Pd back-donation, CO vibrational frequencies are expected to be much lower. Indeed, for a classical square-planar $Rh(I)(CO)_2$ fragment in zeolite H-FAU (isoelectronic and isostructural with square-

DOI: 10.1021/acs.jpcc.9b06760
J. Phys. Chem. C 2020, 124, 309−321

planar $Pd^{+2}(CO)_2$ with two framework oxygens as ligands), the CO signatures lie at 2117 and 2053 cm^{-1}, below the gas-phase CO value: in this complex, Rh is tightly bound to the framework. DFT provides a remarkable agreement between the calculated and experimental frequencies for this complex.[18,52,54]

Nonclassical metal carbonyls have received attention in the organometallic literature. Due to pioneering efforts coming from the Aubke group,[19−23] for example, it was demonstrated that nonclassical transition-metal carbonyls can be produced from Pd or Pt compounds in toxic/corrosive magic acids HSO_3F/SbF_5 in the absence of moisture and under CO pressures. (As noted by Olah and Klumpp,[44] a variety of cationic species from organocations to metal cations should be called "super electrophilic" due to the labile and weakly coordinating nature of fluorosulfonate or similar weakly coordinating anions produced in the "magic"/superacid); moreover, with the help of NMR spectroscopy, the organic (carbocationic) isolated super electrophilic species have been identified in magic acids on the basis of their very high shifts in the ^{13}C NMR region, meaning that extremely positive "super electrophilic" carbocations form under such conditions; however, the super electrophilicity of metal ions/fragments has not been ever proved or quantified before—below, we show that we can now quantify it with XPS for the first time.) For example, $Pd^{+2}(CO)_2(SO_3F)_2$ was obtained, in which $Pd^{+2}(CO)_2$ fragments were weakly interacting with the anion. On the basis of single-crystal XRD data, $Pd^{+2}(CO)_2$ fragments were proposed to stabilize via secondary contacts of CO with basic SO_3F groups dispersed in the crystallographic structure. These compounds were stable only in the complete absence of moisture and decomposed immediately in the presence of traces of water or above 130 °C. The frequencies of the υ_{sym} and υ_{asymm} vibrational features were observed at 2220 and 2199 cm^{-1} (in solution). Note that the split between these two bands is identical to that previously assigned to Pd(III)-$(CO)_2$.[11,12] Thus, we may reassign the 2214 and 2193 cm^{-1} signatures to $Pd^{+2}(CO)_2$ nonclassical dicarbonyl, charge-balanced by two negative charges associated with Al pairs and weakly interacting with the basic O ions of the zeolite, in principle, similar to $Pd^{+2}(CO)_2(SO_3F)_2$. XPS data (vide infra) (in addition to EXAFS data showing Pd^{+2} in an oxygen environment) confirm this result. The slight red shift from 2220 to 2214 cm^{-1} reflects either a higher basicity of zeolite oxygens compared with that of SO_3F anions or alternatively the effect of confinement. The more correct annotation for this sample would then be a charge-transfer/ion-pair complex between $[Pd(CO)_2]^{2+}$ and two $^{-}$O-zeolite. Indeed, the CO adsorption on the pink-colored $Pd^{2+}(^{-}O\text{-}Zeo)_2$ produces a purple-colored $[Pd(CO)_2]^{2+}(^{-}O\text{-}Zeo)_2$ complex (Figure S5), indicating significant charge transfer in the ∼520 nm UV−vis spectral region of both species. We tried to model this complex with DFT calculations (Table S1 and Figures S6−S9 for the structures of various modeled Pd complexes). The results from DFT calculations show significant disagreement with respect to the observed frequencies and in the split between the CO bands. The calculated CO signatures are 2172 and 2138 cm^{-1} with a 34 cm^{-1} split. However, among all $Pd(CO)_2$ fragments, this is the only one that shows a C−O stretching vibrational feature above that of gas-phase CO. We have also attempted to model the nonclassical complex with the known crystallographic structure (i.e., $Pd^{+2}(CO)_2(SO_3F)_2$). The Pd-$(CO)_2(SO_3F)_2$ structure was optimized, and the calculated frequencies were 2199 and 2164 cm^{-1}, once again lower than the experimental values of 2220 and 2199 cm^{-1}. The calculated split was 35 cm^{-1}, larger than the experimentally measured split of 20 cm^{-1} (the same as for modeled $Pd^{+2}(CO)_2$ in zeolite). Again, these computational estimates give ∼30−40 cm^{-1} lower frequencies than the experiment. We suggest that the nonclassical super electrophilic nature of such Pd complexes complicates their modeling by DFT. However, based on the provided evidence, this Pd/SSZ-13 system selectively forms nonclassical $Pd^{+2}(CO)_2$ fragments and not $Pd^{+3}(CO)_2$ as previously proposed in the literature.[11,12,24,28] The nonclassical nature of this complex is further indirectly corroborated by the fact that its infrared signature does not depend on the zeolite type to any significant extent and presents a $Pd^{+2}(CO)_2$ fragment stabilized as ion pairs (with the Al-associated negative oxygen atoms of zeolite acting as a negative part of the ion pair, whereas Pd^{+2} and $Pd^{+2}(CO)_2$ are the positive +2-charged part of the ion pair) in a small (∼0.85 nm) SSZ-13 cage (Figure S10).[11,12,24] Zeolites with larger cavities do not seem to selectively stabilize this fragment, yet it is observable.[24] In conclusion, semifree nonclassical, super electrophilic, $Pd^{+2}(CO)_2$ is formed in the micropores of SSZ-13 and is probably stabilized by the secondary interactions between its CO ligands and the basic oxygens of the zeolite framework. The interactions of CO fragments with framework sites (stabilization) withdraw it from Al and suggests that it may exist as a semifree $[Pd(CO)_2]^{2+}$ ion weakly interacting with the framework (the framework itself can thus be regarded as a weakly coordinating macroanion). All other nonclassical carbonyl complexes prepared in HSO_3F/SbF_5 exist only in the complete absence of moisture.[19−23] Herein, we demonstrated that a $Pd^{+2}(CO)_2$ nonclassical carbonyl complex is insensitive to the presence of H_2O. The IR spectra (Figures 2 and S11) recorded after the exposure of the $Pd^{+2}(CO)_2$/SSZ-13 to moisture clearly substantiate the remarkable stability of this complex.

The small-pore SSZ-13 structure with ∼0.85 nm diameter cages may not provide the typical "liquid" water environment, which lends unique stability to this complex (Figure S10).

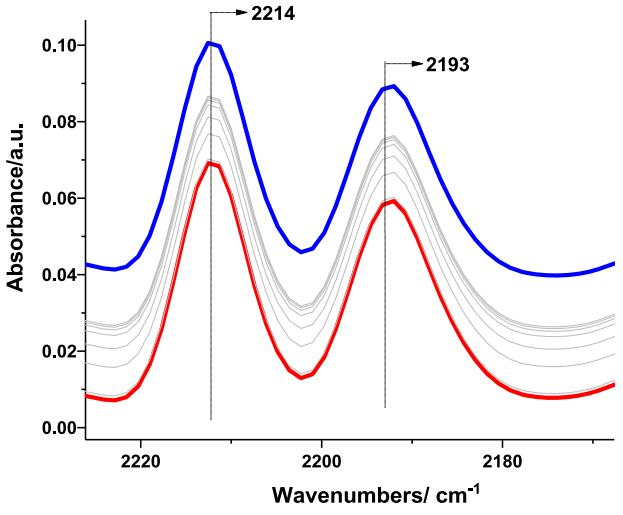

Figure 2. FTIR spectra collected on $Pd^{+2}(CO)_2$/SSZ-13 with Si/Al = 6 upon the adsorption of H_2O at 298 K (H_2O was introduced into the IR cell in a stepwise fashion; $P_{H_2O,\ max}$ ∼6 Torr; sample before H_2O adsorption "dry"—red graph, final state "wet"—blue graph).

DOI: 10.1021/acs.jpcc.9b06760
J. Phys. Chem. C 2020, 124, 309−321

Furthermore, the adsorption of NO pulses on this complex leads exclusively to the formation of $Pd^{+2}(NO)(CO)$, which has been previously characterized in our prior work and identified as the species responsible for the excellent passive NOx adsorber (PNA) performance under practical conditions (Figures S12–S14). (CO and NO uptake curves under practically relevant conditions are displayed in Figure S15, confirming the stoichiometry of the complex in addition to FTIR data in Figures S12 and S14.)[8] Additional experimental evidence of the peculiar chemistry taking place upon dosing only dry NO on Pd(II)/SSZ-13 is provided in Figure S13 and the corresponding discussion in the caption. As we have previously suggested, based on DFT calculations and deduction from experimental data,[8] the 1865 cm^{-1} band belongs to the Pd(II)–NO complex, whereas 1806 cm^{-1} band, which forms upon NO adsorption is due to the reduction of Pd(II) by a free radical NO resulting in the formation of a Pd(I)–NO complex, analogous to what we have shown for the Cu(II)/SSZ-13 system.[65]

The Aubke group has also reported the ability to form a nonclassical $[Pd^{+2}(CO)_4]$ complex under higher CO pressures.[19−23] We have therefore modeled two tetracarbonyl complexes of Pd^{2+} cation and of Pd^0 in the CHA structure (Table S1). Interestingly, in the $Pd^{2+}(CO)_{4zeo}$ complex, the carbon of one of the CO molecules is bound to an oxygen center from the zeolite with a C–O distance of 141 pm. Despite the fact that we were successfully able to model and construct these unusual homoleptic structures, we find no evidence that they are formed under our experimental conditions most likely due to kinetic reasons; i.e., high pressures of CO and different temperatures may be required to observe the formation of such completely homoleptic structures.

We extended our work to 1 wt % Pt and 3 wt % Ag in SSZ-13 (Si/Al = 6) as well (Figure S16 for the HAADF-STEM images of 1 wt % Pt/SSZ-13). In Pt/SSZ-13, nonclassical $Pt^{+2}(CO)_2$ with CO frequencies 2186 and 2153 cm^{-1} is formed in addition to two classical Pt^{+2}–CO monocarbonyls (Figure 3). DFT modeling of classical Pt^{+2} monocarbonyl complexes allows us to unambiguously assign the 2133 cm^{-1} band to $Pt^{+2}(CO)$ in the 8-membered ring, whereas the ~2117 cm^{-1} band belongs to $Pt^{+2}(CO)$ in the 6-membered ring (Figure S17 and Tables 2 and S2). These results clearly demonstrate the confinement of isostructural Pt^{+2}–CO, which leads to the downshift of its IR signature. These bands cannot belong to the dicarbonyl species because they grow independently from each other. The fact that 2186 and 2153 cm^{-1} bands change in concert upon evacuation is a clear indication that they belong to the same species, which, analogously with $Pd^{+2}(CO)_2$, can be assigned to $Pt^{+2}(CO)_2$. Surprisingly, DFT modeling found two energetic minima for two isostructural and isoelectronic $Pt^{2+}(CO)_2$ complexes in the 8-membered ring with very similar stabilities but different frequencies (2156 and 2108, and 2179 and 2136 cm^{-1}, respectively). The likely reason for this is that in one of the complexes CO molecules are close to the zeolite framework with O–O distances of 240 pm. This unusual finding that two essentially isoelectronic and isostructural M–CO complexes could have significantly different C–O stretching frequencies is notable.

DFT calculations for $Pt^{+2}(CO)_2$, both in the 6- and 8-membered rings, show a better agreement with respect to the symmetric C–O stretch with the experiment (~2180 cm^{-1}

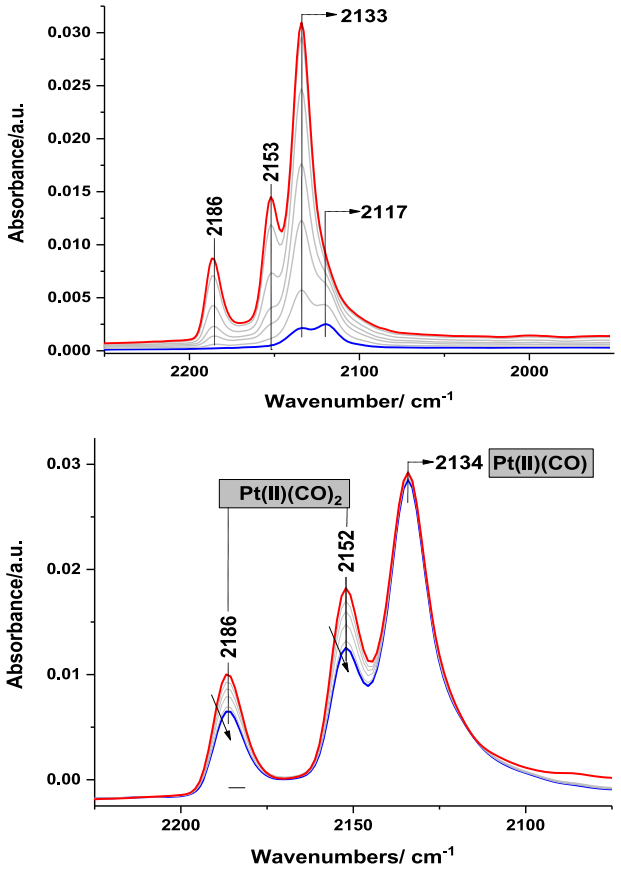

Figure 3. FTIR spectra collected on 1 wt % Pt(II)/SSZ-13 (Si/Al = 6) at P_{CO} = 5 Torr CO pressure (a) and after evacuation (b) at 298 K.

Table 2. Binding Energies of all of the Neutral Ligands (BE, in kJ/mol) and of the Second Adsorbed Ligand (BE_{L2}, in kJ/mol), Vibrational Frequencies of Diatomic (C–O) Ligands (x (L) in cm^{-1}), Pt–Ligand Distances (in pm) (Pt–L), Distances between Pt Cation and Zeolite O Centers (Pt–O_{zeo}), and Number of the Unpaired Electrons in the Systems, N_s

Structures	BE	BE_{L2}	x (L)[a]	d (Pt–L)	d (Pt–O_{zeo})	N_s
Pt^{2+}					206; 206; 212; 212	0
$Pt^{2+}(CO)$	−134		2108	185	208; 211; 211	0
$Pt^{2+}(CO)_2$	−318	−184	2182; 2136	189; 189	209; 209	0
$Pt^{2+}(OH)$				190	202; 210; 211	1
$Pt^{2+}(CO)(OH)$	−181		2146	188; 194	209; 209	1
Pt^{2+} 8-MR					200; 206; 211	0
$Pt^{2+}(CO)$_a 8-MR	−309		2138	186	202; 211; 212	0
$Pt^{2+}(CO)$_b 8-MR	−309		2134	186	202; 211; 213	0
$Pt^{2+}(CO)_2$_a 8-MR	−481	−173	2156; 2108	190; 190	206; 210	0
$Pt^{2+}(CO)_2$_b 8-MR	−479	−170	2179; 2135	189; 190	205; 210	0

[a]The frequencies are shifted by +35 cm^{-1} since the calculated C–O vibrational frequency for a CO molecule in gas-phase 2108 cm^{-1} is lower by 35 cm^{-1} with respect to the experimental value of 2143 cm^{-1}.

DOI: 10.1021/acs.jpcc.9b06760
J. Phys. Chem. C 2020, 124, 309−321

both), although the asymmetric C−O stretch at 2135/2136 cm^{-1} is much lower than that of the observed 2153 cm^{-1}. Moreover, the observed experimental frequencies for $Pt^{+2}(CO)_2$ are below those of $Pd^{+2}(CO)_2$, which is in perfect agreement with the observation by Aubke group, with the split between the band for $Pt^{+2}(CO)_2$ (34 cm^{-1}) larger than for $Pd^{+2}(CO)_2$ (21 cm^{-1}).[19−23] Thus, the formation of the nonclassical $Pt^{+2}(CO)_2$ fragment is confirmed. Although the intensities of the bands belonging to classical Pt monocarbonyls are higher than for the $Pt^{+2}(CO)_2$ species, due to the aforementioned significantly higher molar extinction coefficients of CO complexes with downshifted vibrational frequencies, the Pt^{+2}−CO complexes may not be present as the major species.[42,43,53] Moreover, it is important to note that this is the first observation of the $Pt^{+2}(CO)_2$ fragment on a solid support. Nonzeolitic solid support does not seem to provide any evidence for its existence. However, in some previous literature, the $Pt^{+2}(CO)_2$ was claimed to exist in the ZSM-5 zeolite (noteworthy, unlike in our case, metal nanoparticles were always present in those systems alongside cationic Pt sites): in one report by Hadjiivanov and coworkers, the 2165 and 2150 cm^{-1} bands with the split between them equal to 15 cm^{-1} were assigned to $Pt^{+2}(CO)_2$;[55] interestingly, the bands at 2204 and 2168 cm^{-1} in Y-zeolite[56] (in another report by the same group at 2211 and 2175 cm^{-1} in ZSM-5,[55] correspondingly) were assigned to $Pt^{+3}(CO)2$. Based on our new understanding of the system, it is highly unlikely that Pt^{+3} ions would be present in ZSM-5 or Y with a Si/Al ratio of 10−15 due to the fact that this would require three Al sites to be in very close proximity either in the same ring or in the nearby rings (although it is possible, statistically, their amount would be very low). In those works, the observed split ∼34−35 cm^{-1} corresponds exactly to the split we observe for the $Pt^{+2}(CO)_2$ fragment confined in SSZ-13. Thus, the signatures assigned to $Pt^{+3}(CO)_2$ in previous works with a split between CO bands of 34−35 cm^{-1} have to be reassigned to $Pt^{+2}(CO)_2$. The 2165 and 2150 cm^{-1} assigned previously to $Pt^{+2}(CO)_2$, thus, belong to some other Pt carbonyl complexes and not $Pt^{+2}(CO)_2$.

A comparison of calculated and experiment bands for various observed Pd and Pt complexes is summarized in Table 3.

In the case of Ag/SSZ-13, nonclassical silver $[Ag(CO)]^{+1}$ with a C−O stretch at 2186 cm^{-1} and, at higher CO pressures (>1 Torr), nonclassical $[Ag(CO)_2]^{+1}$ species with a C−O stretch at 2177 cm^{-1} are also formed in SSZ-13 at room temperature (Figure 4).[25,26,45] This is in excellent agreement with the work by the Strauss group.[25,26,45] Indeed, they found that the Ag^{+1} salt of the weakly coordinating anion $[Nb(OTeF_5)_6]^-$ can form $Ag(CO)^+$ and $Ag(CO)_2^+$ with CO signatures of 2208 and 2198 cm^{-1}, respectively, in good agreement with the CO split between mono- and dicarbonyl Ag complexes in SSZ-13. Only under pressures above 13 atmospheres could the authors observe the formation of $[Ag(CO)_3]^{+1}$. Similarly to Pt and Pd, the CO stretches with Ag in the confined microvoids of SSZ-13 are downshifted.

These complexes do not decompose in the presence of significant amounts of water, signifying a general trend for SSZ-13 to stabilize such complexes selectively with remarkable stability in the presence of water (Figure 5).

The nonclassical nature of the $Pd^{+2}(CO)_2$ cation also explains why its vibrational frequencies are similar for a range of zeolites. The unique 0.85 nm in diameter cavity in SSZ-13

Table 3. Comparison between Calculated (υ_{calc}) and Experimental (υ_{exp}) CO and NO Frequencies (in cm^{-1}) in the Complexes of Pd^+, Pd^{2+}, and Pt^{2+} Cations Located in the Zeolite

structures	υ_{calc} (L)[a]	υ_{exp}
$Pd^+(NO)$	1804	1805
$Pd^{2+}(CO)$	2114	2110
$Pd^{2+}(CO)_2$	2172; 2138	2214; 2193
$Pd^{2+}(NO)$	1843	1865
$Pd^{2+}(CO)(NO)$	2146/1830	2150/1800
$Pd^{2+}(CO)(OH)^e$	2121	2133−2147
$Pd^{2+}(CO)(C_2H_4)$	2140	2140
$Pd^{2+}(NO)(C_2H_4)$	1807	1774
$Pt^{2+}(CO)$ (in 6-MR)	2108	2118
$Pt^{2+}(CO)$_a (in 8-MR)	2138	2133
$Pt^{2+}(CO)$_b (in 8-MR)	2134	2133
$Pt^{2+}(CO)_2$_a (in 8-MR)	2156; 2108	2186; 2153
$Pt^{2+}(CO)_2$_b (in 8-MR)	2179; 2135	2186; 2153

[a]The C−O vibrational frequencies are shifted by +35 cm^{-1} since the calculated C−O vibrational frequency for a CO molecule in gas-phase 2108 cm^{-1} is lower by 35 cm^{-1} with respect to the experimental value, 2143 cm^{-1}.

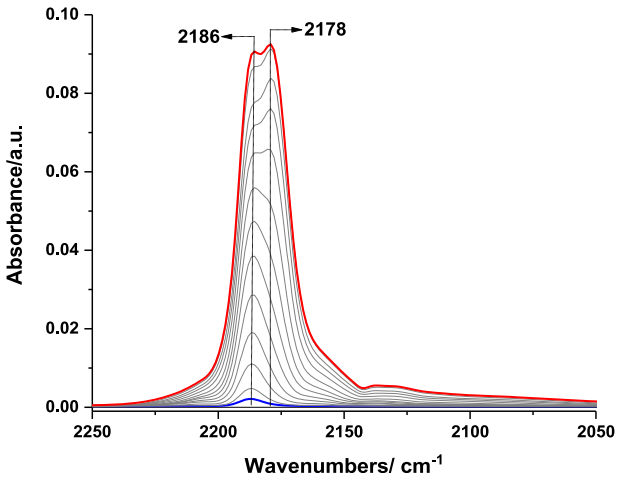

Figure 4. FTIR spectra recorded from 3 wt % Ag/SSZ-13 (Si/Al = 6) during stepwise CO adsorption ($P_{CO,\ max.}$ = 10 Torr).

seems to be a great stabilizer for such species. Its additional charge-transfer character is also evident based on the intense pink-purple color of the complex upon CO adsorption (Figure S5). Previous studies claimed the formation of Pd(IV) cation on various solid supports and zeolites based on (1) the indirect evidence from stoichiometry from XRD refinement,[27] (2) DFT modeling,[46] and (3) the presence of the high binding energy feature (relative to PdO with BE of Pd $3d_{5/2}$ at 336.5−337.0 eV) in the Pd 3d XPS spectra.[24,28,29,47,48] Interestingly, in some works, a feature at 337.7−338.0 eV on ceria supports, for example,[49−51] was attributed to Pd(IV) ions or PdO_2. Therefore, to clarify this issue and provide complementary evidence to the FTIR-based conclusions, we performed quasi in situ XPS (Figures S18−S26) and high-resolution XPS measurements (Figures S25 and S26) on the samples with 0.1 and 1 wt % Pd on SSZ-13 (Si/Al = 6). It is very important to note that for both 0.1 wt % and 1 wt % Pd/SSZ-13 Si/Al ∼6 samples, the two lower-lying BE (binding energy) peaks of Pd $3d_{3/2}$ and $3d_{5/2}$, belonging to one species, selectively disappear after dehydration and form only two high-lying BE Pd $3d_{3/2}$

DOI: 10.1021/acs.jpcc.9b06760
J. Phys. Chem. C 2020, 124, 309−321

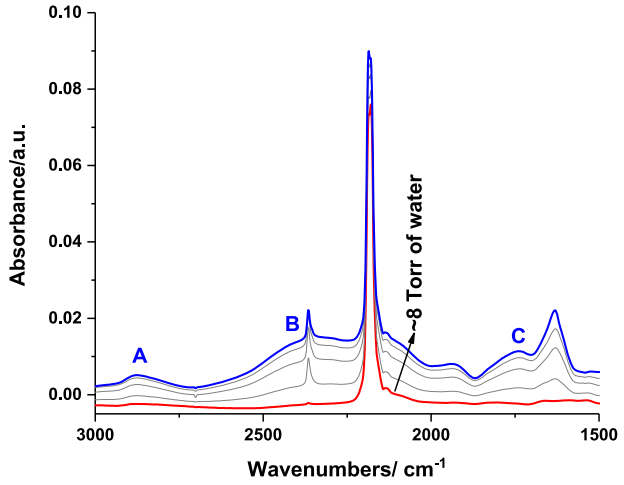

Figure 5. Series of FTIR spectra recorded during the stepwise H_2O exposure ($P_{H_2O,\ max.}$ = ~8 Torr) of Ag−CO/SSZ-13 (Si/Al = 6) sample: Ag(CO) and $Ag(CO)_2$ are stable in the presence of water (while the typical ABC structure of water in the zeolite appears upon water adsorption) at 298 K.[59]

and $3d_{5/2}$ bands belonging to the other species (Figures S25 and S26). For both Pd loadings, the Pd $3d_{5/2}$ feature was shifted by about 2.7 eV compared to typical PdO and over 2.3 eV for Pd^{+2} XPS features observed for typical Pd hydrated or tetramine compounds. At first glance, this seems to indicate a significantly different oxidation state of Pd compared to that of typical Pd^{+2}. Thus, we decided to explore the XPS of 0.1 and 1 wt % Pd/SSZ-13 (Si/Al = 6) in greater detail (Tables S3 and S4, Figures S16−S24). Both feature atomically dispersed Pd as evidenced by the previous HAADF-STEM, EXAFS, XRD, FTIR, and DFT data.[8−10] We also note that upon dehydration either in He or O_2, the color of the sample changes from light yellow to light pink (Figure S3). This is due to the Pd interaction with water vapor. (It is known that water can interact with the Pd ions in the zeolite (analogous to Cu/SSZ-13) and it actually decreases its propensity to interact with the NO molecules. This is why, for example, water can inhibit the performance of such materials in PNA applications in the presence of just NO.[9]) These visual changes for Pd/SSZ-13 happen at the same temperature (~220 °C) both in dry He or O_2. Upon cooling, the pink color is preserved in the absence of moisture—as soon as air/moisture contact takes place, the yellowish color resumes. High-resolution XPS shows two resolved Pd $3d_{5/2}$ peaks both for 1 and 0.1 wt % Pd samples (in the presence of moisture in the air). Their corresponding binding energies are 337.3 and 339.6 eV. The low-lying peak is near where the Pd^{+2} hydrated cations typically show up and higher than highly dispersed PdO.[29] The high-lying peak (2.3 eV higher) could potentially be attributed to Pd in a higher oxidation state. The peaks demonstrate reproducible behavior upon heating: more specifically, the low-energy peak disappears and completely transforms into the high-energy peak for both 0.1 and 1 wt % Pd.

This could indicate two things: the transformation of Pd^{+2} into the Pd ions with a higher oxidation state or the removal of water coordinated to some of the Pd cations and subsequent transformation to the Pd^{+2} sites with unusually high binding energy (BE). In the case of Rh prepared from $Rh(CO)_2(Acac)$ and anchored as $Rh(CO)_2$ classical fragments strongly bound to the HY framework, a single $Rh(I)(CO)_2$ is upshifted by 1 eV compared to the parent $Rh(CO)_2$ and about ~25 cm^{-1} in the FTIR spectra, a notably high value.[30,31] The zeolite, thus, indeed may act as a macroligand in whose cages/micro-channels the complex sits. However, the 2.3 eV shift is exceptionally high. The possibility where Pd^{+2} is oxidized to Pd(IV) can only be envisioned via the formation of $(O_{zeolite})_2$−Pd(IV)═O (Table S1) with an unprecedented Pd═O bond (since it is impossible to have four Al atoms in the realistic vicinity of Pd(IV) or three Al atoms near Pd(IV)−OH). The formation of a compound with Pd(IV)═O bond is definitely a possibility, and in this case, this would be the first case of a Pd complex with a Pd═O oxo bond: indeed, despite many attempts to prepare oxo Pd compounds, all of them have failed so far. However, our previously published XANES data[8] for samples calcined in O_2 directly shows that the overwhelming majority of Pd remains in the +2 oxidation state due to the absence of typical features for Pd(IV).[14] Furthermore, in the case of 1 wt.% Pd, one could argue that some PdO may be visible, but for 0.1 wt % Pd/SSZ-13, all Pd should be 100% atomically dispersed. Thus, the lower binding energy (BE) XPS feature belongs to either fully or, more likely, partially hydrated Pd cations in zeolite: such cations have the typical yellow color characteristic of mononuclear $[Pd^{+2}(H_2O)_4]$ or $[Pd^{+2}(NH_3)_4]$ cations. However, we do not believe that they are fully hydrated Pd ions, but likely Pd^{+2} cations with one or potentially two H_2O molecules adsorbed onto them (or inserted between the framework and Pd^{+2}, which breaks up the $Pd^{+2}/2\ ^{-}O_{zeolite}$ ion pair). Indeed, our DFT calculations demonstrate that the H_2O binding to the Pd cations is favorable (Table S1). Upon heating, we observe water removal from Pd^{+2} and the formation of a light pink Pd−zeolite system with isolated super electrophilic Pd^{+2} cations: their super electrophilic nature is evident based on the extremely high shift of the binding energy of the Pd^{+2} feature by 2.3−339.6 eV compared to the isolated (partially) hydrated Pd(II) ions in the zeolite micropore. This process is reversible, as evidenced by the restoration of the yellow color in the presence of water vapor.

To understand whether unprecedented Pd(IV)═O species could indeed form upon oxidation, and whether the oxidation of Pd(II) was responsible for the color change from yellow to pink, the following experiment was conducted. We produced the pink sample (~300 mg, 1 wt % Pd/SSZ-13), purged it with helium, and reacted it in the oxygen-free glovebox with a minimum amount of deaerated H_2O in a closed vial with a septum. The sample turned yellow. To explain the restoration of the yellow Pd(II)/SSZ-13 upon interaction with water, the reduction of Pd(IV) to Pd(II) in the presence of water ought to take place via the following redox reaction: Pd(IV) + 2e → Pd(II). As Pd accepts two electrons, water has to give electrons, which can only occur by oxidizing H_2O: $H_2O - 2e \rightarrow 2H^+ + 1/2O_2$. If Pd(IV) was reduced to Pd(II), it would produce 14 micromoles of O_2. However, no O_2 was produced; therefore, no reduction took place. Furthermore, if the oxidation of Pd(II) were to take place by heating in the presence of oxygen, then during the sample heating in inert gas, the yellow sample containing hydrated Pd(II) ions would not turn pink (which happens in O_2 as well). Instead, this transformation happens both in inert gas and in oxygen, confirming that no Pd(IV) is produced. Thus, Pd remains in the +2 oxidation state, and changes in the electrophilicity of Pd(II) ions upon water adsorption/desorption are responsible for the observed color variation. Therefore, we are able to

DOI: 10.1021/acs.jpcc.9b06760
J. Phys. Chem. C 2020, 124, 309−321

quantify super electrophilicity quantitatively with XPS, revealing the selective formation of super electrophilic isolated Pd(II) cations from isolated hydrated Pd(II) cations in the SSZ-13 micropore. Because of the uniformity of 0.1−1 wt % Pd(II) complexes in SSZ-13 with Si/Al ∼ 6 and the selective transformation of hydrated Pd(II) species into one type of super electrophilic dehydrated Pd(II) species, we were able to fully unravel the unique state of the as-formed Pd(II) species and directly measure its super electrophilicity, which manifests itself by a very high (>2 eV) shift of the binding energy of the metal cation in the first-shell oxygen ligand environment. This measurement can be extended to other metals in zeolites to understand whether such exceptionally electrophilic species form in other cases, provided only one type of species can be selectively stabilized in a specific zeolite and metal does not change its oxidation state to a significant extent upon dehydration. However, we also showed that the spectroscopic infrared signature of super electrophilic metal ions on solid supports (at least for Pd and Pt) is the formation of unusually stable nonclassical carbonyl complexes with CO bands in the ∼2200 cm^{-1} region.

We also investigated the interaction of the nonclassical $Pd^{+2}(CO)_2$ complex in the SSZ-13 zeolite with ethylene. In many catalytic applications (e.g., automotive exhaust abatement), the active centers can bind a number of adsorbates from the complex gas mixture they are exposed to. Therefore, identifying and characterizing the adsorbed species that can form in Pd/SSZ-13 in a gas mixture containing both CO and a hydrocarbon (e.g., ethylene) are of great interest. The possible formation of olefin complexes, similar to the cation of the Zeise salt, is also of fundamental interest. When the $Pd^{+2}(CO)_2$/SSZ-13 system was exposed to C_2H_4 at ambient temperature, it completely lost its pink color, suggesting the formation of a new complex (Figure S5). The series of FTIR spectra collected *in situ* during the exposure of $Pd^{+2}(CO)_2$ to ethylene show the gradual decrease in intensity of the two dicarbonyl bands (2193 and 2214 cm^{-1}) and the concomitant development of a new, intense feature centered at 2143 cm^{-1} (Figure 6).

These results suggest the selective formation of a $Pd^{+2}(CO)(C_2H_4)$ complex. In fact, this is the first Pd carbonyl−olefin complex observed despite prior attempts to isolate one.[32] Our DFT data are in excellent agreement with this finding, suggesting that a classical $Pd(CO)(C_2H_4)$ (CO stretch below gas-phase CO) complex formed, which is anchored to the framework (Table S1). This is further corroborated by the color change from purple to white upon the first pulses of ethylene (Figure S5).

The CH stretching region shows very weak bands above 3000 cm^{-1} wavenumbers, similar to Zeise's salt C−H stretches, confirming the presence of a $Pd-C_2H_4$ moiety (Figure 7).

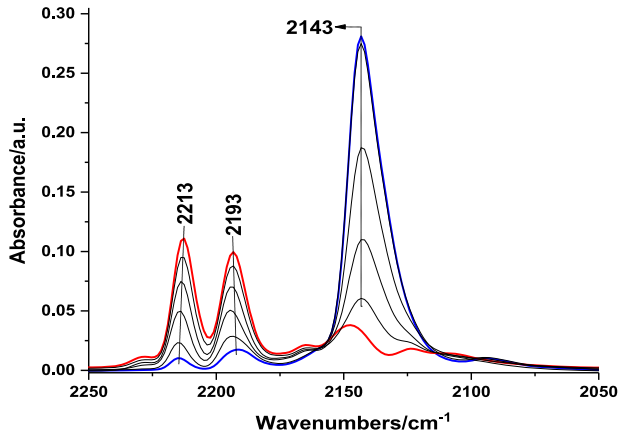

Figure 6. FTIR spectra collected during sequential ethylene adsorption on 1 wt % $Pd(II)(CO)_2$/SSZ-13 (Si/Al = 6) ($P_{C_2H_4,\ max.}$ = 1.5 Torr).

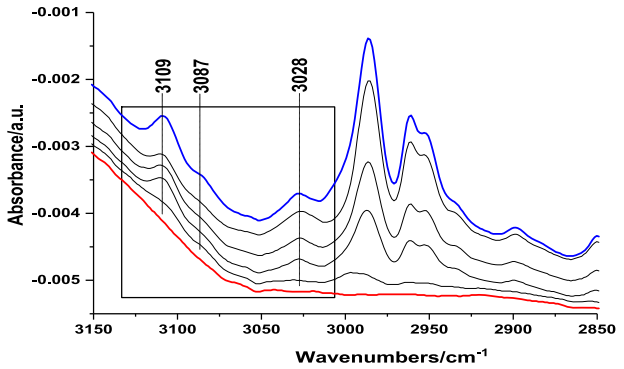

Figure 7. FTIR spectra obtained from $Pd(II)(CO)_2$/SSZ-13 (1 wt % Pd and Si/Al = 6) during sequential ethylene adsorption at 298 K ($P_{C_2H_4,\ max}$ = 2 Torr).

Very similar bands are observed in Rh complexes with pi-ethylene, as well as $Pt^{+2}-C_2H_4$ and $Cu-C_2H_4$ pi-complexes (Figure S27).[33,34] This complex is stable at room temperature and does not decompose under a high vacuum (Figures S28 and S29).

The classical nature of this complex is fully supported by the results of DFT calculations showing an excellent agreement of the calculated C−O stretching frequencies with the experimental ones. The minor shoulder at lower C−O frequencies (2110−2120 cm^{-1}) can be attributed to the $Pd^{+2}(CO)$ species. DFT calculations reveal that CO binding on $Pd^{+2}-CO$ is energetically favorable by 87 kJ/mol, whereas CO binding energy on $Pd(CO)(C_2H_4)$ increases to 151 kJ/mol (almost two times). Comparing the binding energy of ethylene in the $Pd(C_2H_4)$ fragment without CO (58 kJ/mol) to that in the $Pd(CO)(C_2H_4)$ (98 kJ/mol) clearly explains the stability of this fragment. It is of great importance in the context of the so-called passive hydrocarbon traps: the new concept aimed at alleviating hydrocarbon emissions during vehicle cold start. Ethylene binding to naked Pd cations is much weaker than that in the presence of CO (CO is always present in the exhaust), which makes ethylene binding more favorable. Furthermore, ethylene desorption temperature shifts to a higher value, which is beneficial for passive HC trap materials. These results illustrate how the adsorption strength of one adsorbate can be controlled by the presence of a coadsorbate.

Attempts to restore the original $Pd^{+2}(CO)_2$ were unsuccessful (Figure S28) even under elevated CO pressure: we speculate that when the complex is locked in its specific framework-tethered position, it is not possible for it to move back to the nonclassical $[Pd^{+2}(CO)_2]$. However, one may argue that energetics could potentially be responsible for this effect: comparing energies from DFT calculations (Table S1), the adsorption of two CO ligands on Pd^{+2} is exothermic in 215 kJ/mol in electronic energies, whereas the adsorption of CO and C_2H_4 simultaneously is 209 kJ/mol favorable. Although, as we demonstrated earlier, DFT predictions for nonclassical $[Pd^{+2}(CO)_2]$ differ from the real observations, even if we

DOI: 10.1021/acs.jpcc.9b06760
J. Phys. Chem. C 2020, 124, 309−321

assume weaker binding of CO, there should at least be some reversibility of this exchange, which is not observed. Therefore, it is indeed probable that the formation of the locked-in $Pd(CO)(C_2H_4)$ entity bound to the framework strongly prevents its conversion back to nonclassical $[Pd^{+2}(CO)_2]$.

Motivated by the discovery of this mixed carbonyl/ethylene complex of Pd^{+2} in SSZ-13, we set out to investigate the possibility of the formation of other mixed-ligand ethylene complexes. To this end, we exposed a Pd^{+2}–NO complex formed via Pd^{+2}/SSZ-13 interaction with NO to ethylene and observed similar changes in the N–O stretching vibrational region as we have shown above for the carbonyl complex (Figure 8).[35]

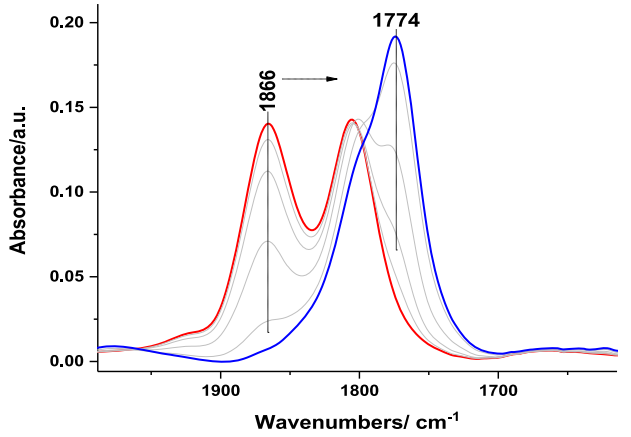

Figure 8. FTIR spectra recorded from Pd–NO/SSZ-13 (1 wt % Pd and Si/Al = 6) during sequential ethylene adsorption at 298 K ($P_{C_2H_4,\ max}$ = 2 Torr).

The band belonging to Pd^{+2}–NO (1865 cm^{-1}) decreased in intensity, while a new N–O stretching vibrational feature developed at 1774 cm^{-1}, indicating the transformation of $Pd^{+2}(NO)$ to $Pd^{+2}(NO)(C_2H_4)$ in the presence of ethylene. This is the first palladium^{+2} nitrosyl/olefin complex observed. The assignment of the new IR band was supported by the results of DFT calculations that predicted a shift of the NO stretching vibrational frequency in the Pd^{+2}–NO complex to lower wavenumbers upon its interaction with ethylene. This resulted in the formation of the $Pd(NO)(C_2H_4)$ complex.

The exposure of the $Pd(NO)(C_2H_4)$ to CO results in the formation of detectable $Pd(CO)(C_2H_4)$ complex, while evacuation restores the Pd(NO) complex (Figures S30 and S35) via ethylene desorption. These results are consistent with the prediction of DFT calculations, i.e., weaker binding of C_2H_4 in the $Pd(NO)(C_2H_4)$ complex compared with $Pd(CO)(C_2H_4)$: C_2H_4 binding energy on nitrosyl complex is 79 kJ/mol, while it is 98 kJ/mol for the carbonyl complex (Table S1). Moreover, Figures S35–S36 provide experimental evidence in addition to Figures S28–S30 for the relative stabilities of the mixed NO–CO–ethylene complexes of Pd(II) in SSZ-13 in agreement with DFT predictions (see the detailed discussion in the captions of Figures S35 and S36).

The changes in the CH stretching region are also very interesting (Figure 9). The low intensity of the C–H stretching band for pi-coordinated ethylene in $Pd(CO)(C_2H_4)$ is as expected since the bands in that region have very low molar extinction coefficients. However, for $Pd(NO)(C_2H_4)$, the C–H stretching region has a higher intensity with bands

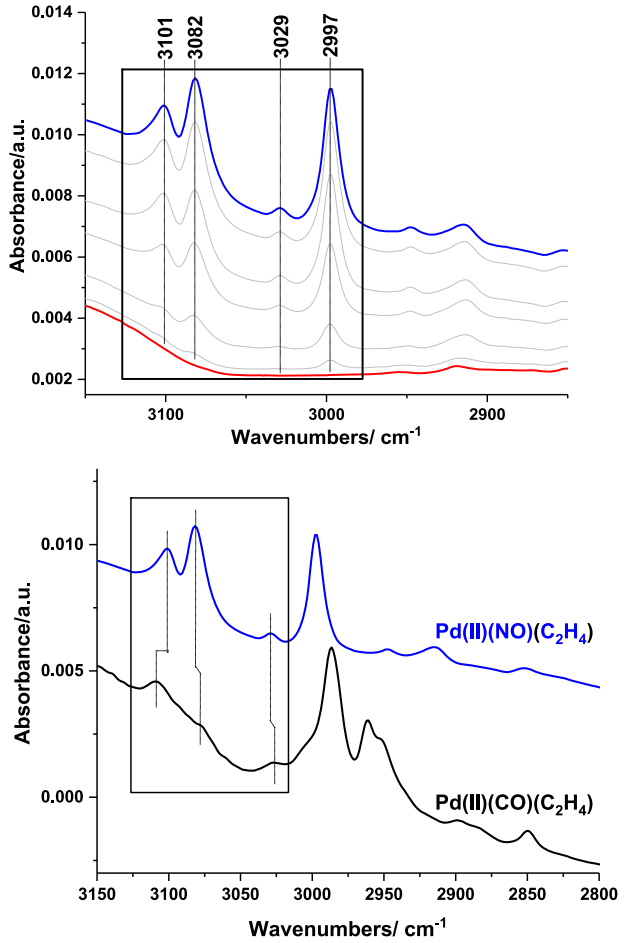

Figure 9. FTIR spectra (in the C–H stretching region) of Pd(II)(NO)/SSZ-13 (1 wt % Pd and Si/Al = 6) during sequential ethylene adsorption (top) and comparison of the same region for $Pd(II)(CO)_2$ exposed to ethylene under identical conditions ($P_{C_2H_4,\ max}$ = 2 Torr).

very different from the ones observed for $Pd^{+2}(CO)(C_2H_4)$ (normalized for both sample preparations).

These differences seem to indicate the catalytic formation of compounds (with specific C–H stretching vibrations) during the exposure of Pd^{+2}NO to ethylene. In contrast, we did not see the development of these features on $Pd(CO)(C_2H_4)$, indicating that the zeolite itself is not responsible for the formation (Figures 7 and S31) of this compound. The developing bands during the exposure of the Pd^{+2}NO complex to ethylene did not match the characteristic features of either polyethylene or butenes. However, when a 5% butadiene/He gas mixture was introduced onto the SSZ-13, bands matching the ones observed after ethylene exposure of the Pd^{+2}NO complex were detected (Figure S32). (These IR features also agree well with the bands reported for butadiene adsorption on various supports.[36−41]) The fact that this reaction can proceed on the $Pd(NO)(C_2H_4)$ but not on the $Pd(CO)(C_2H_4)$ complex indicates a pronounced ligand-directing effect in this catalytic transformation of ethylene to butadiene.

CONCLUSIONS

We synthesized high loadings (1 wt %) of uniform atomically dispersed Pd(II) cations in a small-pore zeolite SSZ-13. Because of the uniformity and selective formation of the

DOI: 10.1021/acs.jpcc.9b06760
J. Phys. Chem. C 2020, 124, 309−321

Pd(II)/2Al species for this material, we were able to unravel their unique chemistry. Previously, their spectroscopic signatures have been assigned to unselectively formed Pd(III) and Pd(IV) species; however, we here show that, in fact, only [Pd(II)//2Al] ions form selectively. We clearly prove that these Pd(II) ions are super electrophilic and quantified super electrophilicity of a metal fragment (ion) for the first time directly with the aid of high-resolution quasi in situ XPS studies (combined with FTIR spectroscopy and DFT calculations). Because in the as-synthesized material in the presence of moisture, water inserts itself between the Pd(II) and basic framework oxygens (associated with the framework Al T-sites), isolated hydrated Pd(II) cations form with a specific XPS signature; they dehydrate selectively forming super electrophilic Pd(II) cations (in the first-shell oxygen ligand environment, as in the case with hydrated Pd(II) cations) whose binding energy (BE) in the 3d Pd XPS spectra shifts to higher BE by exceptional 2.3 eV; thus, this shift is a direct measure of super electrophilicity of a metal fragment. This XPS finding can be potentially extended to other metals in zeolites to probe whether they form super electrophilic species upon dehydration. The highly electrophilic and super electrophilic species formed in zeolites may have great importance for the chemical transformation of organic molecules. The IR signatures upon CO adsorption on super electrophilic metal cations indicate the formation of unusually stable nonclassical carbonyl complexes with CO stretching frequencies in the 2200 cm^{-1} region (2214 and 2193 cm^{-1} in the $Pd(II)(CO)_2$ case).

Thus, such Pd^{+2} ions in SSZ-13 selectively form nonclassical $[Pd^{+2}(CO)_2]$ complexes and Pd(I/II)−NO complexes upon CO and NO adsorptions, respectively. In the presence of both CO and NO, a mixed carbonyl nitrosyl $Pd^{+2}(CO)(NO)$ complex is formed, which has been reported by us previously and which is responsible for the unique performance of Pd ions in SSZ-13 as passive NOx adsorbers. Both $Pd^{+2}(CO)_2$ and $Pd^{+2}(NO)$ can interact with ethylene to form classical palladium carbonyl−olefin $[Pd(CO)(C_2H_4)]$ and nitrosyl−olefin $[Pd(NO)(C_2H_4)]$ complexes, respectively. We also show the first example of comprehensive modeling of a Pd/zeolite (and additionally Pt/zeolite) system including its interactions/activations of small molecules CO, NO, and C_2H_4—these interactions are of great importance for adsorption (e.g., passive NOx adsorbers) and catalysis.

We additionally emphasize the importance of confined nanospace (micropores) of zeolites for the formation of atomically dispersed metal ions with unusually high electrophilicity and, as a consequence, unique physicochemical properties. Out of them, SSZ-13 stands out due to its high hydrothermal stability and thus has great industrial potential, for example, for low-temperature passive NOx adsorption (PNA) applications on the basis of the Pd/SSZ-13 system.

■ ASSOCIATED CONTENT

Supporting Information

The Supporting Information is available free of charge at https://pubs.acs.org/doi/10.1021/acs.jpcc.9b06760.

Additional important discussion, expanded details regarding materials and methods, and 36 figures and 4 tables with XANES region at the Pd K-edge, FTIR spectra under vacuum, XPS data acquisition parameters, cryo-HAADF-STEM images, optimized structures of selected Pd^{2+} complexes, and DFT data (PDF)

■ AUTHOR INFORMATION

Corresponding Authors

*E-mail: Konstantin.Khivantsev@pnnl.gov (K.K.).
*E-mail: Haa@chem.uni-sofia.bg (H.A.A.).
*E-mail: Janos.Szanyi@pnnl.gov (J.S.).

ORCID

Konstantin Khivantsev: 0000-0002-4810-586X
Nicholas R. Jaegers: 0000-0002-9930-7672
Hristiyan A. Aleksandrov: 0000-0001-8311-5193
Libor Kovarik: 0000-0002-2418-6925
Mark Engelhard: 0000-0002-5543-0812
Feng Gao: 0000-0002-8450-3419
Yong Wang: 0000-0002-8460-7410
Janos Szanyi: 0000-0002-8442-5465

Author Contributions

‖K.K., N.R.J., I.Z.K., and J.S. contributed equally to this work.

Notes

The authors declare no competing financial interest.

■ ACKNOWLEDGMENTS

The authors gratefully acknowledge the U.S. Department of Energy (DOE), Office of Energy Efficiency and Renewable Energy, Vehicle Technologies Program for the support of this work. Most of the research described in this paper was performed in the Environmental Molecular Sciences Laboratory (EMSL), a national scientific user facility sponsored by the DOE's Office of Biological and Environmental Research and located at the Pacific Northwest National Laboratory (PNNL). PNNL is operated for the US DOE by Battelle. H.A.A. and I.Z.K. acknowledge financial support by the Bulgarian Science Fund (project DFNI-T02/20). The computational work was supported by the European Regional Development Fund and the Operational Program "Science and Education for Smart Growth" under contract UNITe No. BG05M2OP001-1.001-0004-C01 (2018−2023).

■ REFERENCES

(1) Sachtler, W. M. H. Zeolite-supported transition metal catalysts by design. *Catal. Today* **1992**, *15*, 419−429.
(2) Schweizer, A. E. Noble Metal Alkaline Zeolites for Catalytic Reforming. U.S. Patent US49924011991.
(3) Klier, K. Transition-metal ions in zeolites: the perfect surface sites. *Langmuir* **1988**, *4*, 13−25.
(4) Lónyi, F.; Kovács, A.; Szegedi, A.; Valyon, J. Activation of Hydrogen and Hexane over Pt,H-Mordenite Hydroisomerization Catalysts. *J. Phys. Chem. C* **2009**, *113*, 10527−10540.
(5) Corma, A.; García, H. Crossing the Borders Between Homogeneous and Heterogeneous Catalysis: Developing Recoverable and Reusable Catalytic Systems. *Top. Catal.* **2008**, *48*, 8−31.
(6) Haruta, M. When Gold Is Not Noble: Catalysis by Nanoparticles. *Chem. Rec.* **2003**, *3*, 75−87.
(7) Barrer, M. R. Zeolite Synthesis: An Overview, Surface Organometallic Chemistry: Molecular Approaches to Surface Catalysis, 1998, *221−244*, NATO ASI Series, volume 231.
(8) Khivantsev, K.; Jaegers, N. R.; Kovarik, L.; Hanson, J. C.; Tao, F. F.; Tang, Y.; Zhang, X.; Koleva, I. Z.; Aleksandrov, H. A.; Vayssilov, G. N.; Wang, Y.; Gao, F.; Szanyi, J. Achieving Atomic Dispersion of Highly Loaded Transition Metals in Small-pore Zeolite SSZ-13: a New Class of High-capacity and High-efficiency Low Temperature

DOI: 10.1021/acs.jpcc.9b06760
J. Phys. Chem. C 2020, 124, 309−321

CO and Passive NOx Adsorbers. *Angew. Chem., Int. Ed.* **2018**, *26*, 383−387.
(9) Khivantsev, K.; Gao, F.; Kovarik, L.; Wang, Y.; Szanyi, J. Molecular Level Understanding of How Oxygen and Carbon Monoxide Improve NO x Storage in Palladium/SSZ-13 Passive NO x Adsorbers: The Role of NO+ and Pd +2(CO)(NO) Species. *J. Phys. Chem. C* **2018**, *122*, 10820−10827.
(10) Khivantsev, K.; Jaegers, N. R.; Kovarik, L.; Prodinger, S.; Derewinski, M. A.; Wang, Y.; Gao, F.; Szanyi, J. Palladium/Beta zeolite passive NOx adsorbers (PNA): Clarification of PNA chemistry and the effects of CO and zeolite crystallite size on PNA performance. *App. Catal., A* **2019**, *569*, 141−148.
(11) Aylor, A.; Lobree, L. J.; Reimer, J.; Bell, A. Investigations of the Dispersion of Pd in H-ZSM-5. *J. Catal.* **1997**, *172*, 453−462.
(12) Chakarova, K.; Ivanova, E.; Hadjiivanov, K.; Klissurski, D.; Knozinger, H. Co-ordination chemistry of palladium cations in Pd-H-ZSM-5 as revealed by FTIR spectra of adsorbed and co-adsorbed probe molecules (CO and NO). *Phys. Chem. Chem. Phys.* **2004**, *6*, 3702−3709.
(13) Moliner, M.; Gabay, J. E.; Kliewer, C. E.; Carr, R. T.; Guzman, J.; Casty, G. L.; Serno, P.; Corma, A. Reversible Transformation of Pt Nanoparticles into Single Atoms inside High-Silica Chabazite Zeolite. *J. Am. Chem. Soc.* **2016**, *138*, 15743−15750.
(14) Kim, S.-J.; Lemaux, S.; Demazeau, G.; Kim, J.-Y.; Choy, J.-H. X-Ray absorption spectroscopic study on $LaPdO_3$. *J. Mater. Chem.* **2002**, *12*, 995−1000.
(15) Aleksandrov, H. A.; Neyman, K. M.; Hadjiivanov, K.; Vayssilov, G. N. Can the state of platinum species be unambiguously determined by the stretching frequency of an adsorbed CO probe molecule? *Phys. Chem. Chem. Phys.* **2016**, *18*, 22108−22121.
(16) Aleksandrov, H. A.; Neyman, K. M.; Vayssilov, G. N. The structure and stability of reduced and oxidized mononuclear platinum species on nanostructured ceria from density functional modeling. *Phys. Chem. Chem. Phys.* **2015**, *17*, 14551−14560.
(17) Rivallan, M.; Seguin, E.; Thomas, S.; Lepage, M.; Takagi, N.; Hirata, H.; Thibault-Starzyk, F. Platinum Sintering on H-ZSM-5 Followed by Chemometrics of CO Adsorption and 2D Pressure-Jump IR Spectroscopy of Adsorbed Species. *Angew. Chem., Int. Ed.* **2010**, *49*, 785−789.
(18) Khivantsev, K.; Vityuk, A.; Aleksandrov, H. A.; Vayssilov, G. N.; Alexeev, O. S.; Amiridis, M. D. Effect of Si/Al Ratio and Rh Precursor Used on the Synthesis of HY Zeolite-Supported Rhodium Carbonyl Hydride Complexes. *J. Phys. Chem. C* **2015**, *119*, 17166−17181.
(19) Hwang, G.; Wang, C.; Bodenbinder, M.; Willner, H.; Aubke, F. The syntheses and vibrational spectra of bis(carbonyl)platinum(II) fluorosulfate and bis(carbonyl)palladium+2 fluorosulfate. *J. Fluorine Chem.* **1994**, *66*, 159−166.
(20) von Ahsen, B.; Wartchow, R.; Willner, H.; Jonas, V.; Aubke, F. Bis(carbonyl)platinum+2 Derivatives: Molecular Structure of cis-$Pt(CO)_2(SO_3F)_2$, Complete Vibrational Analysis of cis-$Pt(CO)_2Cl_2$, and Attempted Synthesis of cis-$Pt(CO)_2F_2$. *Inorg. Chem.* **2000**, *39*, 4424−4432.
(21) Willner, H.; Bodenbinder, M.; Brochler, R.; Hwang, G.; Rettig, S. J.; Trotter, J.; von Ahsen, B.; Westphal, U.; Jonas, V.; Thiel, W.; Aubke, F. Superelectrophilic Tetrakis(carbonyl)palladium+2 and platinum: Syntheses, Physical and Spectroscopic Properties, Their Crystal, Molecular, and Extended Structures, and Density Functional Calculations: An Experimental, Computational, and Comparative Study. *J. Am. Chem. Soc.* **2001**, *123*, 588−602. Changqing Wang/Helge Willner/Matthias Bodenbinder/Raymond J. Batchelor/.
(22) Einstein, F. W. B.; Aubke, F.; et al. Formation of cIs-Bis(carbonyl)palladium+2 Fluorosulfate, cIs-$Pd(CO)_2(SO_3F)_2$, and Its Crystal and Molecular Structure. *Inorg. Chem.* **1994**, *33*, 3521−3525.
(23) Hwang, G.; Wang, C.; Aubke, F.; Willner, H.; Bodenbinder, M. The syntheses and vibrational spectra of tetrakis(carbonyl) palladium +2 and platinum+2 undecafluorodiantimonate(V), $[Pd(CO)_4][Sb_2F_{11}]_2$, and $[Pt(CO)_4][Sb_2F_{11}]_2$. *Can. J. Chem.* **1993**, *71*, 1532−1536.
(24) Zheng, Y.; Kovarik, L.; Engelhard, M. H.; Wang, Y.; Wang, Y.; Gao, F.; Szanyi, J. Low-Temperature Pd/Zeolite Passive NOx Adsorbers: Structure, Performance, and Adsorption Chemistry. *J. Phys. Chem. C* **2017**, *121*, 15793−15803.
(25) Hurlburt, P. K.; Anderson, O. P.; Strauss, S. H. Ag(CO)B-$(OTeF_5)_4$: the first isolable silver carbonyl. *J. Am. Chem. Soc.* **1991**, *113*, 6277−627.
(26) Hurlburt, P. K.; Rack, J. J.; Dec, S. F.; Anderson, O. P.; Strauss, S. H. Bis(carbonyl)silver tetrakis(pentafluorooxotellurato)borate: the first structurally characterized $M(CO)_2$ complex. *Inorg. Chem.* **1993**, *32*, 373−374.
(27) Lee, S. H.; Kim, Y.; Seff, K. Crystal Structure of Partially Pd^{2+}-Exchanged Zeolite X Dehydrated in Oxygen at 400 °C. Formation of Linear Pd_2O_3 Clusters Proposed to Be HO-Pd^{IV}-O-PdIV-OH. *J. Phys. Chem. B* **2000**, *104*, 2490−2494.
(28) Mihai, O.; Trandafilovic, L.; Wentworth, T.; Torres, F. F.; Olsson, L. The Effect of Si/Al Ratio for Pd/BEA and Pd/SSZ-13 Used as Passive NOx Adsorbers. *Top. Catal.* **2018**, *61*, 2007−2020.
(29) Kim, K. S.; Gossmann, A. F.; Winograd, N. X-ray photoelectron spectroscopic studies of palladium oxides and the palladium-oxygen electrode. *Anal. Chem.* **1974**, *46*, 197−200.
(30) Khivantsev, K.; Vityuk, A.; Aleksandrov, H. A.; Vayssilov, G. N.; Alexeev, O. S.; Amirdis, M. D. Effect of Si/Al Ratio and Rh Precursor Used on the Synthesis of HY Zeolite-Supported Rhodium Carbonyl Hydride Complexes. *J. Phys. Chem. C* **2015**, *119*, 17166−17181.
(31) Khivantsev, K. Selective Synthesis and Characterization of Single-Site HY Zeolite-Supported Rhodium Complexes and Their Use as Catalysts for Ethylene Hydrogenation and Dimerization. Ph.D. Thesis; University of South Carolina, 2015.
(32) Rix, F. C.; Brookhart, M.; White, P. S. Mechanistic Studies of the Palladium+2-Catalyzed Copolymerization of Ethylene with Carbon Monoxide. *J. Am. Chem. Soc.* **1996**, *118*, 4746−4764.
(33) Hübner, G.; Rauhut, G.; Stoll, H.; Roduner, E. Ethyne Adsorbed on CuNaY Zeolite: FTIR Spectra and Quantum Chemical Calculations. *J. Phys. Chem. B* **2003**, *107*, 8568−8573.
(34) Grogan, M. J.; Nakamoto, K. Infrared Spectra and Normal Coordinate Analysis of Metal-Olefin Complexes. I. Zeise's Salt Potassium Trichloro (ethylene) platinate +2 Monohydrate. *J. Am. Chem. Soc.* **1966**, *88*, 5454−5460.
(35) Khivantsev, K.; Vityuk, A.; Aleksandrov, H. A.; Vayssilov, G. N.; Blom, D.; Alexeev, O. S.; Amirdis, M. D. Synthesis, Modeling, and Catalytic Properties of HY Zeolite-Supported Rhodium Dinitrosyl Complexes. *ACS Catal.* **2017**, *7*, 5965−5982.
(36) Parker, S. F.; Carias, C.; Tomkinson, J. Vibrational spectra of buta-1,3-diene iron tricarbonyl: comparison to surface species. *Catal. Struct. React.* **2017**, *3*, 119−127.
(37) Wu, Z.; Hao, Z.; Ying, P.; Li, C.; Xin, Q. An IR Study on Selective Hydrogenation of 1,3-Butadiene on Transition Metal Nitrides: 1,3-Butadiene and 1-Butene Adsorption on Mo_2N/γ-Al_2O_3 Catalyst. *J. Phys. Chem. B* **2000**, *104*, 12275−12281.
(38) Hisatsune, I. C. Infrared spectra of 1,3-butadiene matrices containing some atomic metals. *Spectrochim. Acta, Part A* **1984**, *40*, 391−395.
(39) Jing, Z.; Weicheng, W.; Shiyang, L. In Situ IR Spectroscopic Study on the Hydrogenation of 1,3-Butadiene on Fresh Mo_2C/γ-Al_2O_3 Catalyst. *China Pet. Process. Petrochem. Technol.* **2014**, *16*, 32−37.
(40) Silvestre-Albero, J.; Borasio, M.; Rupprechter, G.; Freund, H.-J. Combined UHV and ambient pressure studies of 1,3-butadiene adsorption and reaction on Pd(111) by GC, IRAS and XPS. *Catal. Commun.* **2007**, *8*, 292−298.
(41) Voskoboinikov, T. V.; Coq, B.; Fajula, F.; Brown, R.; McDougall, G.; Couturier, J. L. An in situ diffuse reflectance FTIR study of the cyclodimerization of 1,3-butadiene over Cu-exchanged zeolites. *Microporous Mesoporous Mater.* **1998**, *24*, 89−99.
(42) Ding, K.; Gulec, A.; Johnson, A. M.; Schweitzer, N. M.; Stucky, G. D.; Marks, L. D.; Stair, P. C. Identification of active sites in CO oxidation and water-gas shift over supported Pt catalysts. *Science* **2015**, *350*, 189−192.

DOI: 10.1021/acs.jpcc.9b06760
J. Phys. Chem. C 2020, 124, 309−321

(43) Hadjiivanov, K. I.; Vayssilov, G. N. Characterization of oxide surfaces and zeolites by carbon monoxide as an IR probe molecule. *Adv. Catal.* **2002**, *47*, 307−511.
(44) Olah, G. A.; Klumpp, D. A. Superelectrophilic Solvation. *Acc. Chem. Res.* **2004**, *37*, 211−220.
(45) Rack, J. J.; Moasser, B.; Gargulak, J. D.; Gladfelter, W. L.; Hochheimer, H. D.; Strauss, S. H. Infrared and manometric evidence for the formation of the $[Ag(CO)_3]^+$ complex ion at high P(CO). *J. Chem. Soc., Chem. Commun.* **1994**, 685−686.
(46) Gannouni, A.; Delbecq, F.; Zina, M. S.; Sautet, P. Oxidation of Methane to Methanol over Single Site Palladium Oxide Species on Silica: A Mechanistic view from DFT. *J. Phys. Chem. A* **2017**, *121*, 5500−5508.
(47) Gannouni, A.; Rozanska, X.; Albela, B.; Zina, M. S.; Delbecq, F.; Bonneviot, L.; Ghorbel, A. Theoretical and experimental investigations on site occupancy for palladium oxidation states in mesoporous Al-MCM-41 materials. *J. Catal.* **2012**, *289*, 227−237.
(48) Reifsnyder, S. N.; Otten, M. M.; Henry Lamb, H. Nucleation and growth of Pd clusters in mordenite. *Catal. Today* **1998**, *39*, 317−328.
(49) Pozdnyakova, O.; Teschner, D.; Wootsch, A.; Kröhnert, J.; Steinhauer, B.; Sauer, H.; Toth, L.; Jentoft, F. C.; Knop-Gericke, A.; Paál, Z.; Schlögl, R. Preferential CO oxidation in hydrogen (PROX) on ceria-supported catalysts, part II: Oxidation states and surface species on Pd/CeO2 under reaction conditions, suggested reaction mechanism. *J. Catal.* **2006**, *237*, 17−28.
(50) Guimarães, A. L.; Dieguez, L. C.; Schmal, M. Surface Sites of $Pd/CeO_2/Al_2O_3$ Catalysts in the Partial Oxidation of Propane. *J. Phys. Chem. B* **2003**, *107*, 4311−4319.
(51) Meng, L.; Lin, J. J.; Pu, Z. Y.; Luo, L. F.; Jia, A. P.; Huang, W. X.; Luo, M. F.; Lu, J. Q. Identification of active sites for CO and CH_4 oxidation over $PdO/Ce_{1-x}Pd_xO_{2-1}$ catalysts. *Appl. Catal., B* **2012**, *119*, 117−122.
(52) Goellner, J. F.; Gates, B. C.; Vayssilov, G. N.; Rösch, N. Structure and bonding of a site-isolated transition metal complex: Rhodium dicarbonyl in highly dealuminated zeolite Y. *J. Am. Chem. Soc.* **2000**, *122*, 8056−8066.
(53) Hadjiivanov, K.; Chakarova, K.; Drenchev, N.; Mihaylov, M. Characterisation of Porous Materials by FTIR Spectroscopy of Isotopically Labelled Probe Molecules. *Curr. Phys. Chem.* **2012**, *2*, 151−161.
(54) Vayssilov, G. N.; Rösch, N. A new interpretation of the IR bands of supported Rh (I) monocarbonyl complexes. *J. Am. Chem. Soc.* **2002**, *124*, 3783−3786.
(55) Chakarova, K.; Mihaylov, M.; Hadjiivanov, K. FTIR spectroscopic study of CO adsorption on Pt−H−ZSM-5. *Microporous Mesoporous Mater.* **2005**, *81*, 305−312.
(56) Chakarova, K.; Hadjiivanov, K.; Atanasovaa, G.; Tenchev, K. Effect of preparation technique on the properties of platinum inNaY zeolite: A study by FTIR spectroscopy of adsorbed CO. *J. Mol. Catal. A: Chem.* **2007**, *264*, 270−279.
(57) Ryou, Y.-S.; Lee, J.; Lee, H.; Hwan Kim, C.; Heui Kim, D. Effect of various activation conditions on the low temperature NO adsorption performance of Pd/SSZ-13 passive NOx adsorber. *Catal. Today* **2019**, *320*, 175−180.
(58) Lee, J.; Ryou, Y.-S.; Hwang, S.; Kim, Y.; Cho, S.-J.; Lee, H.; Hwan Kim, C.; Heui Kim, D. Comparative study of the mobility of Pd species in SSZ-13 and ZSM-5, and its implication for catalytic activity after hydro-thermal aging as Passive NOx Adsorbers (PNAs) for cold-start applications. *Catal. Sci. Technol.* **2019**, *9*, 163−173.
(59) Claydon, M. F.; Sheppard, N. Nature of "A,B,C"-type infrared spectra of strongly hydrogen-bonded systems; pseudo-maxima in vibrational spectra. *J. Chem. Soc. D* **1969**, 1431−1433.
(60) Khivantsev, K.; Jaegers, N. R.; Kovarik, L.; Hu, J. Z.; Gao, F.; Wang, Y.; Szanyi, J. *Emiss. Control Sci. Technol.* **2019**, 1−13.
(61) Kwak, H.; Tonkyn, R. G.; Kim, D. H.; Szanyi, J.; Peden, C. H. F. *J. Catal.* **2010**, *275*, 187.
(62) Kwak, J. H.; Zhu, H.; Lee, J. H.; Peden, C. H. F.; Szanyi, J. *Chem. Commun.* **2012**, *48*, 4758−4760.
(63) Göltl, F.; Sautet, P.; Hermans, I. *Angew. Chem., Int. Ed.* **2015**, *54*, 7799−7804.
(64) Jaegers, N. R.; Khivantsev, K.; Kovarik, L.; Klas, D.; Hu, J. Z.; Wang, Y.; Szanyi, J. Catalytic activation of ethylene C-H Bonds on uniform D8 Ir(I) and Ni(II) cations in zeolites: toward molecular level understanding of ethylene polymerization on heterogeneous catalysts. *Catal. Sci. Technol.* **2019**, *9*, 6570−6576.
(65) Kwak, J. H.; Lee, J. H.; Burton, S. D.; Lipton, A. S.; Peden, C. H.; Szanyi, J. A Common Intermediate for N_2 Formation in Enzymes and Zeolites: Side-On Cu−Nitrosyl Complexes. *Angew. Chem., Int. Ed.* **2013**, *52*, 9985−9989.

DOI: 10.1021/acs.jpcc.9b06760
J. Phys. Chem. C 2020, 124, 309−321